AGU PUBLICATIONS

JGR

Journal of Geophysical Research: Planets

RESEARCH ARTICLE
10.1002/2013JE004553

Special Section:
Results from the first 360 Sols of the Mars Science Laboratory Mission: Bradbury Landing through Yellowknife Bay

This article is a companion to *Litvak et al.* [2014] doi:10.1002/2013JE004556.

Key Points:
- First analysis of active neutron data from DAN instrument on board MSL rover
- Estimations of water distribution along MSL rover traverse by DAN instrument
- Estimations of chlorine abundance along MSL rover traverse by DAN instrument

Correspondence to:
I. G. Mitrofanov,
mitrofanov@l503.iki.rssi.ru

Citation:
Mitrofanov, I. G., et al. (2014), Water and chlorine content in the Martian soil along the first 1900 m of the Curiosity rover traverse as estimated by the DAN instrument, *J. Geophys. Res. Planets*, *119*, 1579–1596, doi:10.1002/2013JE004553.

Received 9 OCT 2013
Accepted 18 JUN 2014
Accepted article online 21 JUN 2014
Published online 15 JUL 2014

Water and chlorine content in the Martian soil along the first 1900 m of the Curiosity rover traverse as estimated by the DAN instrument

I. G. Mitrofanov[1], M. L. Litvak[1], A. B. Sanin[1], R. D. Starr[2], D. I. Lisov[1], R. O. Kuzmin[1,3], A. Behar[4], W. V. Boynton[5], C. Hardgrove[6], K. Harshman[5], I. Jun[4], R. E. Milliken[7], M. A. Mischna[4], J. E. Moersch[6], and C. G. Tate[6]

[1]Department of Nuclear Planetology, Institute for Space Research of Russian Academy of Science, Moscow, Russia, [2]Department of Physics, Catholic University, Washington, D.C., USA, [3]Comparative Planetology Laboratory, V.I. Vernadsky Institute of Geochemistry and Analytic Chemistry of Russian Academy of Science, Moscow, Russia, [4]Jet Propulsion Laboratory/California Institute of Technology, Pasadena, California, USA, [5]Department of Planetary Sciences, University of Arizona, Tucson, Arizona, USA, [6]Department of Earth and Planetary Sciences, University of Tennessee, Knoxville, Tennessee, USA, [7]Department of Geological Sciences, Brown University, Providence, Rhode Island, USA

Abstract The presence of hydrated phases in the soil and near-surface bedrock of Gale Crater is thought to be direct evidence for water-rock interaction in the crater in the ancient past. Layered sediments over the Gale Crater floor are thought to have formed in past epochs due to sediment transport, accumulation, and cementation through interaction with fluids, and the observed strata of water-bearing minerals record the history of these episodes. The first data analysis of the Dynamic Albedo of Neutrons (DAN) investigation on board the Curiosity rover is presented for 154 individual points of active mode measurements along 1900 m of the traverse over the first 361 Martian solar days in Gale crater. It is found that a model of constant water content within subsurface should be rejected for practically all tested points, whereas a two-layer model with different water contents in each layer is supported by the data. A so-called direct two-layer model (water content increasing with depth) yields acceptable fits for odometry ranges between 0 and 455 m and beyond 638 m. The mean water (H_2O) abundances of the top and bottom layers vary from 1.5 to 1.7 wt % and from 2.2 to 3.3 wt %, respectively, while at some tested spots the water content is estimated to be as high as ~5 wt %. The data for odometry range 455–638 m support an inverse two-layer model (water content decreasing with depth), with an estimated mean water abundance of 2.1 ± 0.1 wt % and 1.4 ± 0.04 wt % in the top and bottom layers, respectively.

1. Introduction

Water ice is not stable on the surface of Gale Crater in the current Martian climate, but H_2O or OH molecules, hereafter referred to as "water," may exist in the chemical structure of hydrated minerals or adsorbed on the surface of the regolith grains. Different locations along the crater floor could contain more or less water in the subsurface depending on variations in local geology and mineralogy, which in turn reflect differences in conditions of water accumulation, water-rock interaction, and erosion. Locations with more water could be the most promising for testing the conditions of habitability and preservation potential on Mars because water is a key ingredient for life, and many hydrated minerals are known to favor preservation of biosignatures. Understanding the distribution of water in the near surface of Gale Crater will also help us to understand the origin, evolution, and diagenetic history of sedimentary deposits in the crater. These two objectives have motivated the measurements of water content in the shallow subsurface on board the Mars Science Laboratory (MSL) rover [*Grotzinger et al.*, 2012].

DAN (Dynamic Albedo of Neutrons) is a Russian-contributed instrument on MSL [see *Litvak et al.*, 2008; *Mitrofanov et al.*, 2012] that addresses the need for these measurements. It uses a method of active neutron sensing of the shallow subsurface. DAN has a pulsing neutron generator (PNG) that produces 2 μs pulses of 14.1 MeV neutrons at a frequency of 10 Hz, with about 10^7 particles in each pulse. The high-energy neutrons penetrate into the subsurface and follow a random walk through interactions with soil and bedrock nuclei, changing direction and decreasing in energy at each interaction (i.e., the diffusion of neutrons takes place in

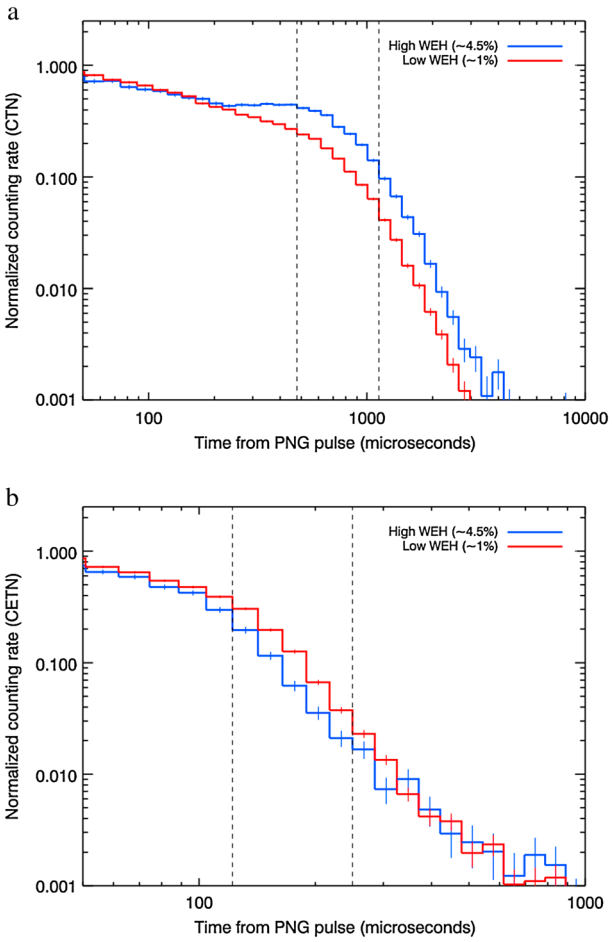

Figure 1. Examples of measured time profiles of postpulse emission for thermal neutrons (Figure 1a) and epithermal neutrons (Figure 1b). Blue and red profiles correspond to testing spots at the driest and the wettest area with odometry 486.9 m and 1075.73 m, respectively (see Table 2). Twelve time intervals selected for water concentration estimation are shown between dashed vertical lines.

the subsurface and is accompanied by a moderation of their energies). A large fraction of neutrons leak out from the surface and produce the *dynamic albedo of neutrons* (hence the name of the DAN instrument). The postpulse emission of these albedo neutrons takes place during a time interval varying from several hundred microseconds up to several milliseconds. Due to the random character of moderation of individual leaking particles, the flux of postpulse neutrons has a broad energy distribution from an upper limit that corresponds to the initial energy of the injected neutrons (14.1 MeV) down to the thermal energy 0.04(300/*T*) eV (where *T* is temperature in kelvin). The lower energy range corresponds to the thermal equilibrium energy ~3/2 *kT* of the soil. The efficiency of the moderation process is known to depend on the presence of hydrogen in the target material because during a neutron-hydrogen collision the light nucleus of the hydrogen atom (a proton) takes about the same recoil energy as the scattered neutron. Increasing hydrogen content results in more thermal neutrons (and, correspondingly, less epithermal or higher energy, neutrons) leaking from the surface.

DAN has two ^{3}He proportional counters to detect epithermal and thermal neutrons (see *Mitrofanov et al*. [2012] for details). The counter of epithermal neutrons (CETN) has a Cd enclosure. It is sensitive to epithermal neutrons with energies above the threshold of ~0.4 eV, because Cd has a very large absorption cross section for neutrons with energies below this value. The counter of thermal neutrons (CTN) detects both thermal and epithermal neutrons. Therefore, one may derive counts for the thermal neutrons (in the energy range below 0.4 eV) by subtracting counts of the CETN detector (counting epithermal neutrons) from counts of the CTN detector (counting a sum of thermal and epithermal neutrons). These detectors measure thermal and epithermal albedo of neutrons from many neutron pulses to get the average time profiles of postpulse emission. They are measured as average count rates in 64 time bins after the start time of the initial pulse, which are spaced over the full time between successive pulses (See section 2 and Figure 1). The shape of the measured time profiles depends on the hydrogen content in the irradiated subsurface and on the vertical distribution of hydrogen-bearing phases in the soil or bedrock. Hydrogen in the Martian soil is primarily associated with water; thus, active neutron sensing allows us to study the lateral and vertical (subsurface) distribution of water and hydrated minerals. Some moderated neutrons can also be absorbed by nuclear capture reactions, which also affect the postpulse time profiles. In the Martian regolith, chlorine and iron are known to be the main nuclei with large neutron capture cross sections [*Hardgrove et al*., 2011], the presence of which should be taken into account in the analysis of active neutron sensing data.

This paper is focused on the first analysis of the DAN active data set, but DAN can also operate in a passive mode of neutron measurement that does not require use of the PNG. The passive neutron measurements made by DAN on MSL characterize the *stationary albedo* of the soil for neutrons from two different sources:

nuclear cascades in the subsurface due to GCRs and irradiation by the rover Multi-Mission Radioisotope Thermoelectric Generator (MMRTG) [see *Mitrofanov et al*., 2012]. The initial interpretation of DAN passive data is presented by *Jun et al*. [2013].

It is important to note that the active neutron sensing data do not provide direct measurements of the water content of the subsurface. DAN measures neutrons postpulse emission, which depends on the hydrogen abundance, which in its turn depends on the presence of H_2O/OH in the irradiated subsurface. To estimate the concentration and distribution of water at a particular location, one has to perform a deconvolution of the neutron data to find the best model fit to the observations (see details in *Litvak et al*. [2014]). This procedure is based on Monte Carlo simulations of time profiles of leaking thermal and epithermal neutrons for different soil models with varying composition, density, and vertical distribution of hydrogen. Calculated time profiles are compared to the measured profiles, and the best fit parameters are determined by using the Pearson's χ^2 test. The results can be considered as the experimental estimations of the water-related parameters of the soil derived from direct measurements of active neutron sensing. The estimated concentration of hydrogen is typically converted into water equivalent hydrogen (WEH) by taking into account that two hydrogen atoms are linked with one oxygen. In theory one may consider a specific hydrated mineral(s) with known numbers of OH and/or H_2O in the chemical formula. In this case abundances of these species could be calculated from known WEH values. Here we assume no specific OH or H_2O-bearing mineral structures in the subsurface and instead estimate WEH as the main parameter for assessing variations in bulk water content of the Martian soil.

2. DAN Active Measurements

Between 17 August 2012 and 12 August 2013, DAN performed 193 individual active measurements in 154 unique locations along the first 1900 m of the MSL traverse path from the landing site. An individual testing spot has a diameter of irradiation of ~3 m and a sensing depth of about 60 cm [see *Litvak et al*., 2014]; therefore, one particular active measurement characterizes the average water content of about 4 m^3 of Martian soil and/or rock below the rover. For one active measurement, the DAN PNG produces pulses at a frequency of 10 Hz for 5 or 15 min depending on the observation. As noted above, the instrument sensors measure the postpulse emission of thermal and epithermal neutrons as a function of time within 64 time bins, with $t = 0$ at the moment of the pulse. The total number of counts is integrated within each bin during the measurement, and time profiles of postpulse counts represent the average counting rate for each of the time bins (Figure 1).

For the first 361 Martian solar days (sols), the DAN PNG produced about $1.3 \cdot 10^{13}$ neutrons, each with energy of 14.1 MeV, and DAN sensors have recorded about 10^7 albedo neutrons that have been moderated/thermalized in the subsurface. On average, in a typical individual measurement of 15 min, about $9 \cdot 10^4$ neutrons are recorded. This total number yields good statistical confidence of the measured time profiles of postpulse emission both for epithermal and thermal neutrons (see Figure 1). Both neutron profiles clearly decay with time down to the level of the local background neutron count rate. The decay times vary from spot to spot depending on the local composition, but on average they are about 2 ms and 5 ms for epithermal and thermal neutrons, respectively. This time-dependent measurement of postpulse emission is a well-known method of active neutron sensing. The late time intervals on the postpulse time scale provide information on the local background flux of neutrons. Subtracting the count rate values for these late time intervals from the postpulse profiles yields the pure die-away curves of neutron albedo. Such curves, $C_{tn}(t_i)$ and $C_{etn}(t_i)$ for thermal and epithermal neutrons, respectively, in the 64 time bins along the postpulse scale are the observational products from each active measurement [see also *Litvak et al*, 2014].

Before one may use these curves for estimates of subsurface properties at different testing spots, the data must be reduced to account for instrument effects such as variations of the neutron pulse intensity and changes of the sensors efficiency after provision of high voltage (see *Litvak et al*. [2014] and *Jun et al*. [2013] for details). It is known that pulse amplitude varies slightly from pulse to pulse and, even more importantly, slowly decreases over the lifetime of the instrument. Numerical simulations have shown that DAN CTN and CETN counting rate measured in the earliest time bins of the postpulse emission does not significantly depend on Martian regolith properties but is dominated by initial high-energy neutrons backscattered inside the rover mechanical structures close to the detectors and/or neutron generator. Making evident assumption that rover properties does not change during surface operations, one may remove the instrumental effects, provided the measured die-away time profiles of counts of neutron albedo, $C_{tn,etn}(t_i)$, are normalized to the

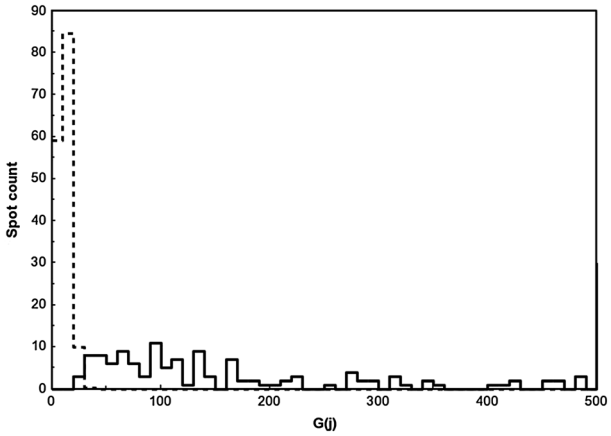

Figure 2. Distribution of the values of $G^{(j)}_{\mathrm{tn,etn}}$, which represent the difference between the measured postpulse profiles and the average curves. The expected distribution of χ^2 with 12 degrees of freedom is shown by dashed line.

same values of count rate in the earliest bins $<50\,\mu$s [*Litvak et al.*, 2014]. These normalized time profiles $A_{\mathrm{tn,etn}}(t_i)$, measured for each testing spot should be compared with the simulated time profiles, $F_{\mathrm{tn,etn}}(t_i, MG)$, calculated for some model group, *MG*, describing particular type of subsurface.

However, the normalized time profiles of recorded counts of neutron albedo still contain a contribution of neutrons that have interacted not only with the soil but also with the mass of the rover. One may assume that the mass of the rover works like an additional reflection element for leaking neutrons. One may use the time-dependent curves, $R_{\mathrm{tn,etn}}(t_i)$, to take into account the increase of counts in each bin of the simulated die-away curves, $F_{\mathrm{tn,etn}}(t_i, MG)$, due to neutron backscattering in the rover body [*Litvak et al.*, 2014]. Thus, for each testing spot the measured normalized time profiles $A_{\mathrm{tn,etn}}(t_i)$ should be compared to the set of simulated curves given as $W_{\mathrm{tn,etn}}(t_i, MG) = R_{\mathrm{tn,etn}}(t_i) \cdot F_{\mathrm{tn,etn}}(t_i, MG)$.

Not all time bins of the normalized time profiles of postpulse emission should be used for testing the simulated curves. The early time bins should be excluded because they are dominated by backscattering on the rover. The late time bins should also not be used for two reasons: the first being that they represent the decay part of the die-away curve with small counting statistics and the second being that the "late" albedo neutrons are arriving from the most distant ring within the irradiated spot and with small angles to the surface. The effect of absorption by the rover itself is the strongest for these neutrons, and minor leaks in the Cd shielding of the CETN neutron detector tend to destroy the signal from some of such directions. It was shown by *Litvak et al.* [2014] that the best signal-to-noise condition for water detection takes place when data from the medium time bins are used for experimental time profiles, $A_{\mathrm{tn,etn}}(t_i)$ (see Figure 1). There are seven and five selected time bins for time profiles $A_{\mathrm{tn}}(t_i)$ and $A_{\mathrm{etn}}(t_i)$, respectively, which provides 12 random variables for testing the models. Therefore, the measurements for each testing spot *j* correspond to the set of variables $\left\{A^{(j)}_{\mathrm{tn,etn}}(t_i)\right\}$, which are equal to the normalized number of counts in the bin *i* of the time profiles for thermal or epithermal neutrons. The estimated statistical errors $\left\{\sigma^{(j)}_{\mathrm{tn,etn}}(t_i)\right\}$ of these variables are based on the statistics of counts in these bins. Therefore, for each of 154 unique testing spots (rover locations), we have 12 independent measured variables and their errors, which characterize the die-away time profiles of postpulse emission.

3. Searching for the Best Models for DAN Data Analysis

The first step of the data analysis is the test for surface variations: using the observational data for individual testing spots, it is necessary to check whether they are consistent with the hypothesis of *uniform soil properties*. In terms of the theory of statistical analysis of observations, one may consider no soil variability to be the *null hypothesis* along the traverse. To test this hypothesis we estimated the average values $A_{\mathrm{tn,etn}}(t_i)$ of variables $\left\{A^{(j)}_{\mathrm{tn,etn}}(t_i)\right\}$ over the full set of testing spots $\{j\}$. There should be no physical variations between testing spots if functional (1)

$$G^{(j)}_{\mathrm{tn,etn}} = \sum_{i=\varepsilon_1^{\mathrm{tn,etn}}}^{\varepsilon_2^{\mathrm{tn,etn}}} \frac{\left(A^{(j)}_{\mathrm{tn,etn}}(t_i) - A_{\mathrm{tn,etn}}(t_i)\right)^2}{\left(\sigma^{(j)}_{\mathrm{tn,etn}}(t_i)\right)^2} \tag{1}$$

corresponds to the χ^2 distribution with 12 degrees of freedom (Pearson criterion), where $\varepsilon_1^{\mathrm{etn}}, \varepsilon_2^{\mathrm{etn}}, \varepsilon_1^{\mathrm{tn}}, \varepsilon_2^{\mathrm{tn}}$, are time bins indexes corresponding to the optimal time intervals for each DAN CETN and CTN detectors [see *Litvak et al.*, 2014]. Figure 2 presents the distribution of the values of $G^{(j)}_{\mathrm{tn,etn}}$ for all 154 testing spots. It is evident that this distribution is far from the shape of the χ^2 distribution with 12 degrees of freedom, which

means that values of $G^{(j)}_{tn,etn}$ at different testing spots are not contributed by random fluctuations of the count statistics. These changes are produced by the real physical variations of neutron albedo emission from the upper ~1 m of soil and bedrock along the rover traverse. The goal of the current data analysis is to find the simplest model of the near surface for which changes of model parameters allow us to explain the observed variations of the neutron albedo.

The postpulse emission of thermal and epithermal neutrons depends on the composition and density of the soil ρ, on the content of water in the soil, ξ_W (as the primary hydrogen-bearing substance), and on the actual content of chlorine ξ^{act}_{Cl} (as the major absorber of thermal neutrons). Below, we use only two variable composition parameters: the content of water ξ_W and the thermal neutron absorption equivalent content of chlorine ξ_{Cl} (see below what means *absorption equivalent*). The total fraction of soil constituting elements, beside water and chlorine, is equal to $\left(1-\xi_W-\xi^{act}_{Cl}\right)$. For a particular element A, the relative fraction ξ_A in the soil (without water and chlorine) is determined in respect to $\left(1-\xi_W-\xi^{act}_{Cl}\right)$. Correspondingly, the absolute content of an element A in the soil is equal to $\xi_A\cdot\left(1-\xi_W-\xi^{act}_{Cl}\right)$. For DAN data analysis, the relative fractions of elements A are assumed to correspond to the Martian soil abundance, as measured by Alpha Particle X-Ray Spectrometer (APXS) Mars Exploration Rover (MER): $\xi_A=\xi^0_A$ (see *Brückner et al.* [2008] and *Litvak et al.* [2014] for details).

The variable content of chlorine was proposed by *Hardgrove et al.* [2011] to take into account absorption of thermal neutrons in the soil. However, it is known that chlorine is not the only element, which has large enough cross section for absorption of thermal neutrons (there are also iron, titanium, etc.). For making DAN data analysis, one cannot use the variable contents of all particular absorbing atoms. Instead, we use the single variable parameter, the content of *absorption equivalent chlorine* ξ_{Cl}, for taking into account all absorbers of thermal neutrons [see *Litvak et al.*, 2014].

Physics of introduction of such parameter is the following. The average free path for neutrons absorption L^{-1}_{ab} is presented by the expression (2):

$$L^{-1}_{ab}=n_{Cl}\cdot\sigma_{Cl}+n_W\cdot\sigma_W+\Sigma_A n_A\cdot\sigma_A=\rho\left(\frac{\xi^{act}_{Cl}\cdot\sigma_{Cl}}{\mu_{Cl}}+\frac{\xi_W\cdot\sigma_W}{\mu_W}+\left(1-\xi_W-\xi^{act}_{Cl}\right)\Sigma_A\frac{\xi_A\cdot\sigma_A}{\mu_A}\right) \quad (2)$$

where n_{Cl}, n_W, and n_A are concentrations of chlorine atoms, water molecules, and all other absorbing atoms A in the soil; σ_{Cl}, σ_W, and σ_A are their thermal neutrons absorption cross sections; and μ_{Cl}, μ_W, and μ_A are their masses, respectively. Here the concentration of chlorine atoms corresponds to its actual fraction in the soil $n_{Cl}=\rho\,\xi^{act}_{Cl}/\mu_{Cl}$. To introduce the parameter of the absorption equivalent chlorine ξ_{Cl}, one should represent the average free path L^{-1}_{ab} (see expression (2)) using the variable content of chlorine only and assuming that the relative fractions of all other absorbing atoms ξ_A are equal to the standard fractions of these atoms ξ^0_A in the Martian soil according to APXS MER measurements:

$$L^{-1}_{ab}=\rho\left(\frac{\xi_{Cl}\cdot\sigma_{Cl}}{\mu_{Cl}}+\frac{\xi_W\cdot\sigma_W}{\mu_W}+(1-\xi_W-\xi_{Cl})\Sigma_A\frac{\xi^0_A\cdot\sigma_A}{\mu_A}\right) \quad (3)$$

Using the condition of equality of these two expressions (2) and (3) for ${L_{ab}}^{-1}$, one gets the relationship between the absorption equivalent content of chlorine ξ_{Cl} and the actual content of chlorine ξ^{act}_{Cl}:

$$\xi_{Cl}=\xi^{act}_{Cl}+\frac{1-\xi_W-\xi^{act}_{Cl}}{1-\Sigma_A\alpha_A\xi^0_A}\Sigma_A\alpha_A\left(\xi_A-\xi^0_A\right) \quad (4)$$

where $\alpha_A=\frac{\sigma_A\,\mu_{Cl}}{\sigma_{Cl}\,\mu_A}$.

Expression (4) helps to understand the physical sense of the parameter of absorption equivalent chlorine: it is equal to the actual content of chlorine ξ^{act}_{Cl} plus additions due to the differences of fractions of other absorbing atoms from their standard values according to APXS MER. Provided the relative fractions of other absorbing elements are equal to the APXS MER values, $\xi_{Cl}=\xi^{act}_{Cl}$. Generally speaking, expression (4) may be considered, as the empirical relationship between the unknown values of abundances of chlorine and other neutron absorbing elements. It is based on the known values of ξ_{Cl} and ξ_W, which were found from the DAN data analysis.

Initial studies [see *Hardgrove et al.*, 2011] have shown that in addition to chlorine there would be several other absorbers of thermal neutrons (such as isotopes of Fe, Mn, and Ti), which could be taken into account for the interpretation of DAN measurements. Following similar approach, we may transform the expression (4) into the numerical formula by taking into account only major neutron absorbers. They could be determined using their thermal neutron capture cross sections, the values of abundances, and

standard deviations of abundances according to the APXS MER data [see *Bell*, 2008]. According to this approach, three major contributing isotopes are ^{56}Fe ($\xi(^{56}\mathrm{Fe}) = 11.8 \pm 3.2$ wt %), ^{32}S ($\xi(^{32}\mathrm{S}) = 3.6 \pm 2.7$ wt %), and ^{48}Ti ($\xi(^{48}\mathrm{Ti}) = 0.4 \pm 0.2$ wt %). Keeping in expression (4) the three major additional members, one gets from expression (4) the numerical form, as

$$\xi_{\mathrm{Cl}} = \xi_{\mathrm{Cl}}^{\mathrm{act}} + 1.01 \cdot \left(1 - \xi_W - \xi_{\mathrm{Cl}}^{\mathrm{act}}\right) \cdot \left[0.037 \cdot \left(\xi(^{56}\mathrm{Fe}) - 0.118\right) + 0.013 \cdot \left(\xi(^{32}\mathrm{S}) - 0.036\right) + 0.14 \cdot \left(\xi(^{48}\mathrm{Ti}) - 0.004\right)\right] \tag{5}$$

It is evident from the expression (5) that absorption equivalent parameter ξ_{Cl} could be quite close to the actual value $\xi_{\mathrm{Cl}}^{\mathrm{act}}$ for the chlorine. Indeed, using the measured standard deviations for abundances of Fe, S, and Ti for the corresponding differences $\left(\xi_A - \xi_A^0\right)$ (see expressions (4) and (5)), one finds out the contributions of these elements, as 0.0012, 0.0004, and 0.0003, respectively. For the expectable content of chlorine about 0.01, these contributions produce rather small corrections of 12%, 4%, and 3% for this chlorine amount, respectively. However, even with such a small possible difference between the values of ξ_{Cl} and $\xi_{\mathrm{Cl}}^{\mathrm{act}}$, we underline in the text below that our estimation for the chlorine abundance is based on the approximation of the absorption equivalent chlorine, expression (4).

In the absence of additional information one does not know, a priori, whether variations of one, two, or even all three parameters ρ, ξ_W, and ξ_{Cl} are responsible for the observed variations of neutron emission. Therefore, we will follow the standard approach for testing models in which the simplest scenario is tested first, and then more and more complex models are tested, provided that the data do not support simpler ones.

We are using below the Model Groups (*MG*) for data analysis. Each group includes the models that use an identical set of free parameters, the values of which are varied to fit the observations. The observed values, $A_{\mathrm{tn,etn}}^{(j)}(t_i)$, of postpulse neutron emission at testing spot *j* are compared with predictions $W_{\mathrm{tn,etn}}(t_i, MG)$ of the *MG* using the functional (6):

$$\Phi(j, MG) = \sum_{i=\varepsilon_1^{\mathrm{tn,etn}}}^{\varepsilon_2^{\mathrm{tn,etn}}} \frac{\left(A_{\mathrm{tn,etn}}^{(j)}(t_i) - k_{\mathrm{tn,etn}}(MG) \cdot W_{\mathrm{tn,etn}}(t_i, MG)\right)^2}{\left(\sigma_{\mathrm{tn}}^{(j)}(t_i)\right)^2 + \left(k_{\mathrm{tn,etn}}(MG)\right)^2 \cdot \left(\omega_{\mathrm{tn,etn}}(t_i, MG)\right)^2}, \tag{6}$$

where $k_{\mathrm{tn,etn}}(MG)$ are the amplitude scaling factors (see below) and $\omega_{\mathrm{tn,etn}}(t_i, MG)$ is the uncertainty of simulated values $W_{\mathrm{tn,etn}}(t_i, MG)$. The minimum of this function determines the values of the free parameters in the used model group that best fit the observations at testing spot *j*.

The amplitude scaling factors $k_{\mathrm{tn,etn}}(MG)$ should be used for the comparison between the measured and simulated time profiles (expression (6)) because we are not able to simulate exact absolute values of neutron count rate. Indeed, one does not know well enough the rover mass contribution for backscattering or the absolute response function of the sensors to model absolute neutron counts with high precision. Generally speaking, one may fit experimental data at each spot using amplitude scaling value as another free parameter. But in this case the model and the data would be compared using the shape of postpulse profiles only, while the amplitude variations would be excluded from the fitting procedure. This is not ideal because variations in albedo flux are known to be quite sensitive to soil composition. On the other hand, one knows that the relative variations of postpulse neutron emission could be produced with high accuracy for different models. Therefore, we have chosen to select one particular reference testing spot and to find for this spot the amplitude scaling factors, k_{tn} and k_{etn}, that provide the highest match between the sums of measured and simulated counts within selected time bins of time profiles for thermal and epithermal neutrons, respectively. It was found that data at the odometry spot of 7 m agree very well with all tested models (described below); therefore, we have selected this point to estimate the amplitude scaling factors in expression (6). We then multiply the simulated values $W_{\mathrm{tn,etn}}(t_i, MGn)$ by these scaling factors for all other spots to allow direct comparison with the observed values (see expression (6)).

Water content is thought to be the parameter most likely responsible for observed variations of neutron albedo at different testing spots. We define *Model Group 1* (*MG1*) as those models with a standard regolith composition [see *Litvak et al.*, 2014], a fixed volume density of 1.8 g/cm^3, and a fixed content of 1 wt % for the absorption equivalent of chlorine. Only one variable parameter is allowed for *MG1* models, that being the content of water, ξ_W, over the sensing depth of the DAN instrument. Using the function $\Phi(j, MG1)$ of expression (6), the best fitting parameters of the water content $\xi_W^{(*)}(j, MG1)$ are found for each testing spot, *j*, from the condition of the

Table 1. Comparison of Different Models Groups for the Sample of 154 Testing Spots

Groups of Models	Number of Spots for Which Data are Consistent With the Model, and Their Fraction	Estimations of the Content of Water: Average Value and Range	Estimations of the Additional Parameters: Range and Average Value	Probability of Acceptance for All Testing Spots
(1)	(2)	(3)	(4)	(5)
MG1: soil with variable water	40 (26%)	Water (wt %) 1.68 ± 0.31 (1.1–2.2)	–	0%
MG2: soil with variable water and density	52 (34%)	Water (wt %) 1.57 ± 0.37 (0.9–2.9)	Density (g/cm^3): 1.88 ± 0.19 (1.5–2.3)	0%
MG3: soil with variable water and absorption equivalent chlorine	87 (56%)	Water (wt %) 1.78 ± 0.33 (1.0–2.6)	Absorption equivalent chlorine (wt %): 1.22 ± 0.26 (0.75–1.75)	0%
MG4: soil with variable water in two layers and variable absorption equivalent chlorine	152 (99%)	Average water (wt %) 2.33 ± 0.67 (1.0–4.4)	Absorption equivalent chlorine (wt %): 1.16 ± 0.25 (0.75–1.75)	6.1%

minimum of this function. However, *MG1* models with a single variable parameter, ξ_W, may only be accepted as an explanation for an active measurement at an individual testing spot provided the value of the minima is consistent with a χ^2 random distribution having 11 degrees of freedom (12 is the number of measured variables $A^{(j)}_{\mathrm{tn,etn}}(t_i)$ minus 1). This consistency would mean that the difference between observed values and the model predictions are produced by random count statistics. In this study we use a probability value of 1% for acceptance of the best fitting models, which means that according to the χ^2 statistics, the found minimum value of $\Phi(j, MG1)$ for a given testing spot has a probability $>1\%$ of being the result of random deviations of observed counts from the model predictions. For *MG1*, this requirement is satisfied by only 40 locations, which is only 26% of the entire suite of observations (Table 1). The distribution of the best fitting values for water equivalent hydrogen $\xi^{(*)}_W(j, MG1)$ is presented in Figure 3 for these 40 cases. The values fall within the interval (1.1–2.2)% WEH with a mean value $<\xi^{(*)}_W(j, MG1)> = 1.68 \pm 0.31\%$ WEH (see Table 1).

The acceptance of *MG1* for the full set of testing spots may be validated by the Pearson criteria: the distribution of the minima expression (6) found for all testing spots should be compared to the χ^2 statistics with 11 degrees of freedom. It is found that there is a very small probability that this distribution agrees with the χ^2 statistics (in practical terms, it is equal to 0, Table 1). Therefore, while some models of *MG1* might work for individual testing spots, the *MG1* group with a single variable parameter (water content) cannot explain the full set of active measurements at all locations.

The DAN PNG is a point source of high-energy neutrons. The volume density of the soil determines the linear dimension of the irradiated volume and, therefore, the leaking flux of albedo neutrons. The next level of complexity of data modeling can be represented by *Model Group 2* (*MG2*), which allows two fitting parameters: a varying soil volume density and variable water content. The minima of $\Phi(j, MG2)$ were found (expression (6)) to obtain the best fitting parameters for the observed time profiles. We used the same approach to test the *MG2* and other more complex models as was used for testing the simplest model, *MG1*, as described above. In 52 cases (corresponding to 34% of testing spots), *MG2* was able to fit the observations with a confidence higher than 1%. Distributions of the best fitting values of the water content $\xi^{(*)}_W(j, MG2)$ and of the density $\rho^{(*)}(j, MG2)$ are presented in Figures 3 and 4. The distribution of water content is similar to the results based on *MG1*, which means that the introduction of one more variable, the volume density, does not significantly improve or alter the quality of the modeling of water variations (one may see this from the comparison of the mean water contents 1.68 ± 0.31 wt % WEH for *MG1* and 1.57 ± 0.37 wt % WEH for *MG2*, see Table 1). On the other hand, the distribution in the density parameter was found to be rather narrow; the mean value for this parameter 1.88 ± 0.19 g/cm^3 is close to the standard value 1.8 g/cm^3 for Martian soil.

The Pearson criterion provides a zero probability for consistency of the entire set of minima expression (6) for *MG2* with the full set of data for all testing spots (Table 1). Based on this, and given that the *MG2* group does not provide any significant change in the water content compared with

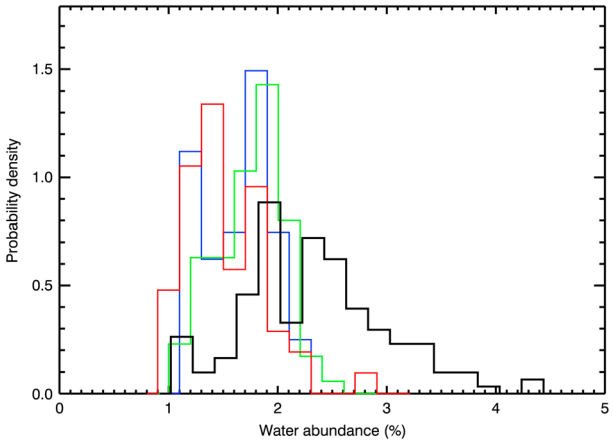

Figure 3. Distributions of estimated contents of water for different Groups of Models: blue line for *MG1*, red line for *MG2*, and green line for *MG3*. The black line corresponds to the average content of water according to the models *MG4*.

MG1, one may conclude that the inclusion of variable density alone does not improve the quality of data modeling. We will therefore use a constant density for the soil, $\rho = 1.8\ \mathrm{g/cm^3}$, for further analysis of the DAN active data.

Model Group 3 (*MG3*), like *MG2*, relies on two variables, but here the parameters are water and absorption equivalent chlorine. One may expect that *MG3* would provide significant improvement of data interpretation because the effect of neutron absorption is known to change the time profile of postpulse emission of thermal neutrons [*Hardgrove et al.*, 2011]. Indeed, there are 87 testing spots for which the data are consistent with the best fit models of *MG3*, having a confidence greater than 1% (which corresponds to 56% of testing spots, see Table 1). Figures 3 and 5 show distributions of the best fitting parameters of these models, such as the content of water $\xi_W^{(*)}(j, MG3)$ and the content of absorption equivalent chlorine $\xi_{\mathrm{Cl}}^{(*)}(j, MG3)$, respectively. The distribution of $\xi_{\mathrm{Cl}}^{(*)}(j, MG3)$ is found to be rather broad, which means that indeed, the observational data requires variations of absorption equivalent chlorine. In contrast, the estimated distribution of the water content using *MG3* is relatively narrow and yields values very similar to the results from *MG1* and *MG2* (Figure 3). Therefore, one can conclude that variations of water and absorption equivalent chlorine are two independent factors contributing to the observed variation of the neutron data.

However, according to the Pearson criteria, the distribution of the minima of values of expression (6) for the full set of testing spots still has a very small probability of being consistent with the random distribution of χ^2 with 10 degrees of freedom. Formal estimations show that the confidence levels of the best fitting models of *MG3* are usually some higher than the levels for models *MG1* and *MG2*, but they are still too small for acceptance (Table 1). Therefore, one cannot use *MG3* for physical interpretation of the observations over the entire sample of testing spots.

The next qualitative level of increasing complexity is *Model Group 4* (*MG4*), which introduces a new kind of variation in water content: two distinct water-bearing layers in the subsurface. One knows that the postpulse time profile of neutron emission is rather sensitive to vertical distribution of hydrogen and, as such, a two-layer model is the simplest approach to take this effect into account. From the data analysis with *MG3* we know that variations of absorption equivalent chlorine are implied by the data; therefore *MG4* should also allow such variations. Instead of the single water parameter, ξ_W, used in groups *MG1–MG3*, the models of *MG4* have two independent parameters of water content for top and bottom layers, $\xi_W^{(\mathrm{top})}$ and $\xi_W^{(\mathrm{bottom})}$, respectively. A third water parameter is the thickness, h, of the top layer. When h is close to zero, the models of *MG4* approach the models of *MG3* with the water content $\xi_W = \xi_W^{(\mathrm{bottom})}$. On the other hand, when h is large enough in comparison with the probing depth, the models of *MG4* correspond to models of

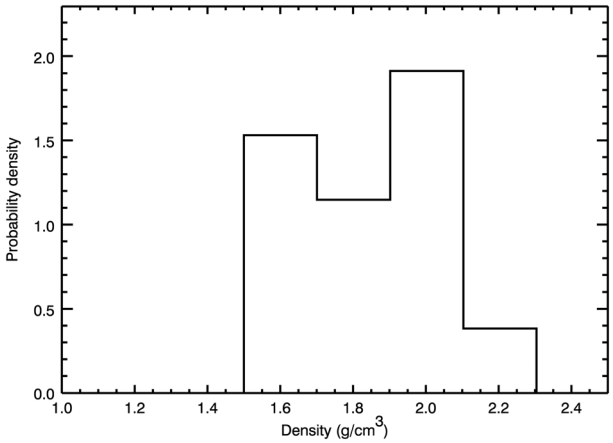

Figure 4. Distribution of estimated density for the models of *MG2*.

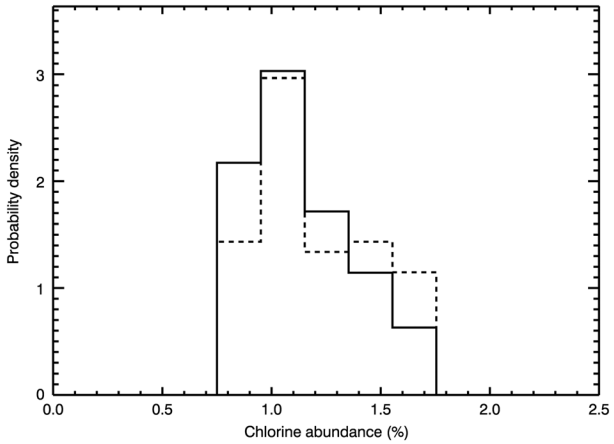

Figure 5. Distributions of absorption equivalent chlorine content for the models *MG3* (dashed line) and *MG4* (solid line).

MG3 with the water content $\xi_W = \xi_W^{(\mathrm{top})}$. The *MG4* group is, thus, physically distinct from *MG3* only in that it can account for vertical changes of the water content in the subsurface sampling depth.

It is found that data for practically all testing spots are well fitted by the two-layer models of *MG4*: 152 spots, or 99%, have a high confidence level >1% for acceptance (see Table 2 for individual fittings parameters of testing spots). To compare fits to the two-layer *MG4* with fits to the single-layer *MG*s 1–3, we introduce a parameter representing the weighted vertical-average water, $\xi_W^{(\mathrm{av})}$, across the two layers, which is testable by the active neutron probing:

$$\xi_W^{(\mathrm{av})} = \frac{h\cdot\xi_W^{(*)(\mathrm{top})} + (H-h)\cdot\xi_W^{(*)(\mathrm{bottom})}}{H}, \tag{7}$$

where H is the thickness of the sensitive testable layer. According to numerical simulations, the sensing depth H of the active neutron probing is assumed to be 60 cm [*Litvak et al*., 2014]. The values $\xi_W^{(\mathrm{av})}$ were calculated for all testing spots that are fitted by *MG4* (Table 2). There is good agreement between these values and those estimated from *MG1–MG3* (Figure 3 and Table 2). The only difference is the tail of the distribution for $\xi_W^{(\mathrm{av})}$ ranges up to 4 wt % WEH in comparison with the limit of 2.3 wt % WEH for models *MG1–MG3*. The reason for this difference is obvious: the single-layer models *MG1–MG3* are able to fit the data when the difference between the top and bottom layers is small and the average water content is about 1–2 wt % WEH These cases are presented in Figure 3. However, data from locations where there exists a large difference in water content between the top and bottom layers are not fit well by *MG1–MG3*, and therefore, they are not represented by corresponding distributions in Figure 3. The two-layer model works well for these cases, and these data correspond to the rightward tail of the distribution for $\xi_W^{(\mathrm{av})}$. Finally, the best fitting values for absorption equivalent chlorine content $\xi_{\mathrm{Cl}}^{(*)}(j, MG4)$ agree quite well with the values derived from the data by *MG*3 (Figure 5). Based on these results one may conclude that the absorption equivalent chlorine content is well-fit by a single-layer model, and it is unnecessary to implement more complex models to account for possible vertical variations in absorption equivalent chlorine content.

The Pearson criteria for the sample of minima values of $\Phi(j, MG1)$ for the best fitting models of *MG4* provide rather good agreement with the χ^2 distribution. The probability for acceptance, 6.1%, is rather good for such a large sample (see Table 2). The agreement of *MG4* with the data is quite good for such a simple, one-step approximation of vertical variations of water in the subsurface. On the other hand, all simpler models (*MG1–MG3*) have small probabilities of acceptance and may fit data from only a portion of the testing spots (Table 1). One may conclude that vertically changing water content is a well-pronounced physical property of the soil, which is required by observations and described by the two-layer models of *MG4*. Therefore, the best fitting parameters of *MG4* are considered below, as the physical evaluations of the water distribution and the absorption equivalent chlorine content in the soil (see Table 2). The notes [(1)] and [(2)] in the column (2) of Table 2 indicate particular testing spots, which are associated with sampling operations at the Rocknest and drilling operations at John Klein and Cumberland (see section 5 below). The note [(3)] indicates the testing spots that were studied as part of a special "DAN campaign" by the MSL rover upon exit from Yellowknife Bay [see *Litvak et al*., 2014].

4. Measured Properties of Soil Along the Traverse

The best fitting parameters of *MG4* for 154 testing spots are presented in Table 2 together with the probability of acceptance of the best fitting model for each individual testing spot. There are only two spots, with odometry distances 109.1 m and 146.1 m, for which data are not fit by the two-layer model. In the other 152 cases the fitting models have probabilities >1% for acceptance.

Table 2. The Best Fitting Parameters of Two-Layer *MG4* Models[a]

Sols	Odometry (m)	Top Water (wt %)	Bottom Water (wt %)	Average Water (wt %)	Top Layer Thickness (cm)	Absorption Equivalent Chlorine (wt %)	Probability of Model Acceptance
(1)	(2)	(3)	(4)	(5)	(6)	(7)	(8)
11–14	0.0	2.20 ± 0.43	1.30 ± 0.14	1.41 ± 0.09	7 ± 8	1.10 ± 0.07	88.4%
17–21	7.0	1.70 ± 0.48	1.10 ± 0.12	1.17 ± 0.07	7 ± 9	1.10 ± 0.08	86.6%
21–22	11.9	1.00 ± 0.49	2.40 ± 0.24	2.35 ± 0.17	2 ± 8	1.40 ± 0.10	4.8%
22–23	27.0	1.70 ± 0.37	1.10 ± 0.12	1.22 ± 0.08	12 ± 7	1.10 ± 0.07	99.7%
24–26	48.5	2.20 ± 0.32	1.50 ± 0.15	1.62 ± 0.09	10 ± 8	1.30 ± 0.09	55.5%
26–29	78.6	3.00 ± 0.47	1.90 ± 0.18	2.03 ± 0.13	7 ± 7	1.20 ± 0.07	7.9%
29–38	109.1	No fitting	No fitting	No fitting	No fitting	No fitting	0.0%
38	141.5	1.20 ± 0.32	2.00 ± 0.25	1.95 ± 0.15	4 ± 9	0.95 ± 0.07	65.3%
39	146.1	No fitting	No fitting	No fitting	No fitting	No fitting	0.2%
39	163.2	1.30 ± 0.20	2.20 ± 0.34	1.75 ± 0.18	**30 ± 7**	0.85 ± 0.09	16.0%
40	200.2	1.60 ± 0.19	2.30 ± 0.31	1.95 ± 0.18	**30 ± 8**	1.05 ± 0.09	1.2%
41	210.2	1.60 ± 0.27	3.00 ± 0.56	2.60 ± 0.37	**17 ± 5**	0.90 ± 0.10	57.5%
41	220.2	1.00 ± 0.55	1.70 ± 0.26	1.60 ± 0.17	9 ± 8	1.10 ± 0.13	18.9%
41	227.4	1.80 ± 0.25	2.70 ± 0.42	2.28 ± 0.25	**28 ± 7**	1.15 ± 0.09	50.2%
42	237.4	1.70 ± 0.25	2.90 ± 0.70	2.52 ± 0.41	**19 ± 6**	1.00 ± 0.10	70.6%
42	247.4	1.80 ± 0.27	2.50 ± 0.54	2.28 ± 0.33	**19 ± 6**	1.00 ± 0.10	78.6%
42	259.4	1.00 ± 0.30	1.90 ± 0.26	1.84 ± 0.15	4 ± 9	1.10 ± 0.08	60.4%
43	279.5	1.10 ± 0.45	2.10 ± 0.32	2.02 ± 0.20	5 ± 8	1.00 ± 0.09	90.4%
43	289.5	2.10 ± 0.42	3.40 ± 0.76	2.97 ± 0.47	**20 ± 6**	1.25 ± 0.11	46.3%
45	293.8	2.10 ± 0.41	1.80 ± 0.21	1.85 ± 0.14	9 ± 8	0.90 ± 0.07	11.9%
48	315.3	2.80 ± 0.50	1.90 ± 0.33	2.01 ± 0.24	7 ± 6	1.05 ± 0.10	13.0%
48	335.8	1.50 ± 0.26	2.00 ± 0.30	1.95 ± 0.17	6 ± 9	1.00 ± 0.08	13.1%
49	351.7	1.00 ± 0.40	2.10 ± 0.37	1.99 ± 0.23	6 ± 9	0.90 ± 0.09	30.5%
50	392.3	1.00 ± 0.57	2.10 ± 0.30	2.01 ± 0.20	5 ± 8	0.95 ± 0.11	27.7%
52	415.5	1.90 ± 0.35	2.60 ± 0.38	2.37 ± 0.24	20 ± 7	1.20 ± 0.10	4.3%
52	453.3	1.00 ± 0.43	2.60 ± 0.41	2.44 ± 0.27	6 ± 8	1.05 ± 0.09	11.4%
54	455.0	2.40 ± 0.32	1.90 ± 0.20	1.97 ± 0.14	8 ± 7	0.95 ± 0.06	63.0%
55	479.1	1.50 ± 0.47	1.10 ± 0.15	1.18 ± 0.10	12 ± 7	1.05 ± 0.09	96.0%
57	485.1[(1)]	3.00 ± 0.72	1.00 ± 0.03	1.03 ± 0.03	1 ± 8	0.95 ± 0.05	7.8%
59	486.9[(1)]	1.70 ± 0.67	1.00 ± 0.04	1.02 ± 0.04	2 ± 7	0.95 ± 0.07	46.7%
72–98	490.0[(1)]	**3.00 ± 0.66**	**1.00 ± 0.01**	1.03 ± 0.02	1 ± 8	0.90 ± 0.04	1.8%
100	491.9[(1)]	1.70 ± 0.46	1.00 ± 0.06	1.04 ± 0.04	3 ± 8	0.80 ± 0.05	21.1%
103–105	517.2	2.40 ± 0.31	1.50 ± 0.14	1.65 ± 0.09	10 ± 6	1.35 ± 0.09	90.0%
111–118	519.1	2.50 ± 0.23	1.80 ± 0.18	1.93 ± 0.13	11 ± 6	1.60 ± 0.08	15.8%
120	545.0	2.70 ± 0.48	1.60 ± 0.23	1.66 ± 0.15	3 ± 8	1.25 ± 0.11	13.3%
120	553.7	2.20 ± 0.45	1.40 ± 0.15	1.44 ± 0.11	3 ± 7	1.25 ± 0.11	52.9%
121	577.9	2.00 ± 0.49	1.20 ± 0.15	1.23 ± 0.10	2 ± 7	1.10 ± 0.10	53.0%
122	578.9	1.80 ± 0.45	1.20 ± 0.14	1.30 ± 0.10	10 ± 7	1.30 ± 0.11	87.1%
123	598.3	2.30 ± 0.33	1.90 ± 0.28	1.97 ± 0.19	10 ± 9	1.55 ± 0.09	77.5%
124	612.3	1.10 ± 0.27	1.90 ± 0.25	1.82 ± 0.16	6 ± 8	1.15 ± 0.11	78.7%
125	638.4	2.30 ± 0.46	1.70 ± 0.19	1.77 ± 0.13	7 ± 7	1.00 ± 0.08	50.9%
127–129	671.2	1.30 ± 0.29	2.00 ± 0.23	1.88 ± 0.13	10 ± 9	1.00 ± 0.07	48.9%
130	676.8	**1.70 ± 0.19**	**3.10 ± 0.40**	2.61 ± 0.25	**21 ± 4**	1.15 ± 0.09	95.7%
133	698.5	1.60 ± 0.22	2.90 ± 0.41	2.51 ± 0.27	**18 ± 4**	1.00 ± 0.09	33.9%
147	701.5	1.70 ± 0.20	2.60 ± 0.36	2.30 ± 0.22	**20 ± 5**	0.95 ± 0.08	79.9%
151	702.2	**1.60 ± 0.25**	**3.30 ± 0.47**	2.79 ± 0.30	**18 ± 4**	1.10 ± 0.09	93.3%
153	704.6	**1.20 ± 0.49**	**3.80 ± 0.67**	3.37 ± 0.41	10 ± 7	1.20 ± 0.09	1.7%
159	705.9	1.70 ± 0.38	1.80 ± 0.23	1.78 ± 0.15	12 ± 9	0.85 ± 0.07	91.2%
163	714.9	1.80 ± 0.26	2.40 ± 0.31	2.20 ± 0.18	20 ± 8	0.95 ± 0.08	45.6%
163	716.8	1.30 ± 0.26	2.00 ± 0.33	1.88 ± 0.19	10 ± 9	0.90 ± 0.08	73.5%
166–267	723.4	1.70 ± 0.17	2.50 ± 0.25	2.23 ± 0.14	**20 ± 5**	1.00 ± 0.08	23.5%
274	726.5	1.40 ± 0.32	1.70 ± 0.20	1.59 ± 0.12	22 ± 8	0.80 ± 0.06	91.6%
276–290	727.2	**1.50 ± 0.11**	**2.60 ± 0.28**	2.05 ± 0.16	**30 ± 5**	0.85 ± 0.07	60.1%
295	729.5[(2)]	**1.10 ± 0.14**	**3.00 ± 0.36**	2.40 ± 0.21	**19 ± 4**	0.80 ± 0.04	74.2%
295	733.5[(2)]	**1.40 ± 0.17**	**2.60 ± 0.35**	2.20 ± 0.21	**20 ± 4**	1.00 ± 0.09	83.3%
297	751.4[(3)]	**1.40 ± 0.14**	**2.70 ± 0.36**	2.29 ± 0.22	**19 ± 5**	0.95 ± 0.07	46.3%
297	752.4[(3)]	1.50 ± 0.20	2.80 ± 0.46	2.30 ± 0.28	**23 ± 5**	1.15 ± 0.12	2.8%
297	753.4[(3)]	1.60 ± 0.21	2.70 ± 0.41	2.28 ± 0.24	**23 ± 6**	1.10 ± 0.09	68.3%
299	754.6[(3)]	**1.20 ± 0.19**	**4.00 ± 0.46**	3.16 ± 0.26	**18 ± 4**	1.20 ± 0.09	49.4%

Table 2. (continued)

Sols	Odometry (m)	Top Water (wt %)	Bottom Water (wt %)	Average Water (wt %)	Top Layer Thickness (cm)	Absorption Equivalent Chlorine (wt %)	Probability of Model Acceptance
299	755.4[(3)]	1.00 ± 0.33	2.10 ± 0.30	2.01 ± 0.18	5 ± 8	1.05 ± 0.08	31.3%
299	756.1[(3)]	**1.50 ± 0.16**	**3.00 ± 0.41**	2.50 ± 0.24	**20 ± 4**	0.90 ± 0.07	34.5%
299	756.9[(3)]	**1.20 ± 0.15**	**2.50 ± 0.35**	2.11 ± 0.20	**18 ± 5**	0.80 ± 0.05	99.1%
299	757.6[(3)]	**1.40 ± 0.12**	**2.50 ± 0.34**	1.97 ± 0.19	**29 ± 5**	0.75 ± 0.04	84.1%
299	758.4[(3)]	**1.40 ± 0.11**	**2.40 ± 0.30**	1.90 ± 0.18	**30 ± 5**	0.80 ± 0.06	82.0%
299	759.1[(3)]	**1.20 ± 0.16**	**4.40 ± 0.53**	3.33 ± 0.30	**20 ± 2**	1.25 ± 0.09	79.3%
299	759.9[(3)]	**1.50 ± 0.15**	**3.20 ± 0.52**	2.63 ± 0.28	**20 ± 4**	1.45 ± 0.11	63.8%
299	760.6[(3)]	**1.30 ± 0.25**	**2.60 ± 0.33**	2.32 ± 0.20	13 ± 6	1.45 ± 0.10	90.4%
299	761.4[(3)]	1.90 ± 0.23	2.80 ± 0.54	2.50 ± 0.32	**20 ± 6**	1.60 ± 0.10	46.5%
299	762.1[(3)]	1.90 ± 0.28	2.70 ± 0.49	2.49 ± 0.26	16 ± 6	1.70 ± 0.11	75.6%
301	762.4[(3)]	1.30 ± 0.31	2.60 ± 0.49	2.38 ± 0.27	10 ± 8	1.40 ± 0.12	65.9%
301	763.2[(3)]	1.00 ± 0.47	2.40 ± 0.37	2.35 ± 0.22	2 ± 9	1.60 ± 0.12	38.4%
301	763.9[(3)]	1.60 ± 0.41	2.40 ± 0.26	2.27 ± 0.17	10 ± 8	1.35 ± 0.12	11.0%
301	764.7[(3)]	1.30 ± 0.34	2.10 ± 0.32	1.97 ± 0.20	10 ± 8	1.15 ± 0.09	67.0%
302	773.7	1.20 ± 0.29	3.30 ± 0.77	2.95 ± 0.42	10 ± 7	1.75 ± 0.08	11.1%
303	776.5	1.50 ± 0.32	3.10 ± 0.73	2.81 ± 0.39	11 ± 6	1.75 ± 0.06	74.0%
307	808.2	3.00 ± 0.45	2.00 ± 0.18	2.02 ± 0.13	1 ± 8	1.70 ± 0.05	8.4%
308	830.2	1.50 ± 0.14	2.70 ± 0.38	2.26 ± 0.22	**22 ± 4**	1.50 ± 0.11	36.3%
309	832.0	2.20 ± 0.34	1.80 ± 0.24	1.87 ± 0.16	10 ± 9	1.50 ± 0.10	21.9%
313	841.3	1.20 ± 0.24	2.20 ± 0.47	2.07 ± 0.26	8 ± 7	1.50 ± 0.14	9.2%
317	848.1	2.00 ± 0.35	1.70 ± 0.21	1.75 ± 0.15	10 ± 8	1.55 ± 0.10	5.7%
324	866.1	**1.30 ± 0.16**	**2.50 ± 0.31**	2.06 ± 0.19	**22 ± 4**	1.15 ± 0.11	41.2%
327	876.1	**1.50 ± 0.28**	**4.40 ± 0.58**	3.58 ± 0.34	**17 ± 4**	1.75 ± 0.07	88.2%
327	888.1	1.20 ± 0.33	1.80 ± 0.33	1.63 ± 0.20	17 ± 8	1.10 ± 0.13	88.5%
327	906.2	1.30 ± 0.21	2.00 ± 0.29	1.65 ± 0.16	**30 ± 7**	0.80 ± 0.07	13.1%
329	916.2	**1.50 ± 0.18**	**4.20 ± 0.71**	3.08 ± 0.44	**25 ± 3**	1.50 ± 0.15	21.0%
329	926.3	1.60 ± 0.34	4.00 ± 0.79	3.32 ± 0.48	**17 ± 5**	1.45 ± 0.14	44.4%
329	936.3	1.40 ± 0.24	3.30 ± 0.71	2.64 ± 0.38	**21 ± 5**	1.15 ± 0.13	30.2%
329	947.3	1.80 ± 0.27	3.40 ± 0.62	2.87 ± 0.34	**20 ± 5**	1.25 ± 0.09	28.3%
331	961.3	1.50 ± 0.47	2.00 ± 0.43	1.93 ± 0.27	9 ± 8	0.85 ± 0.10	59.2%
331	975.3	1.90 ± 0.27	3.20 ± 0.58	2.79 ± 0.32	19 ± 7	1.50 ± 0.11	69.4%
333	982.8	1.20 ± 0.16	2.80 ± 0.59	2.27 ± 0.34	**20 ± 5**	1.15 ± 0.14	59.6%
333	990.8	1.30 ± 0.44	1.50 ± 0.18	1.47 ± 0.13	8 ± 8	1.50 ± 0.10	63.1%
335	1000.0	1.90 ± 0.34	2.30 ± 0.40	2.24 ± 0.27	9 ± 8	1.55 ± 0.10	70.8%
335	1009.0	**1.40 ± 0.23**	**4.10 ± 0.77**	3.20 ± 0.46	**20 ± 3**	1.25 ± 0.12	27.3%
335	1017.0	1.30 ± 0.16	2.80 ± 0.82	2.30 ± 0.43	**20 ± 4**	1.75 ± 0.08	42.7%
335	1025.0	1.60 ± 0.41	1.90 ± 0.36	1.75 ± 0.22	**30 ± 10**	1.15 ± 0.12	90.6%
335	1029.0	1.70 ± 0.39	1.00 ± 0.07	1.13 ± 0.06	11 ± 6	1.10 ± 0.10	87.6%
336	1037.0	1.20 ± 0.21	2.90 ± 0.53	2.45 ± 0.32	**16 ± 4**	0.75 ± 0.03	82.8%
336	1043.0	**1.30 ± 0.14**	**4.00 ± 0.61**	2.65 ± 0.37	**30 ± 4**	0.85 ± 0.12	62.7%
336	1049.0	1.60 ± 0.23	2.40 ± 0.55	2.00 ± 0.33	**30 ± 7**	1.10 ± 0.13	40.1%
336	1055.0	1.70 ± 0.28	3.30 ± 0.58	2.77 ± 0.38	**20 ± 5**	1.10 ± 0.13	32.4%
336	1062.0	**1.90 ± 0.23**	**4.80 ± 0.70**	3.59 ± 0.39	**25 ± 4**	1.35 ± 0.10	11.6%
337	1075.7	**2.70 ± 0.53**	**6.00 ± 0.78**	4.35 ± 0.46	**30 ± 7**	0.75 ± 0.05	71.9%
337	1089.5	1.40 ± 0.23	3.00 ± 0.58	2.47 ± 0.37	**20 ± 5**	0.90 ± 0.12	40.0%
337	1099.6	**1.40 ± 0.16**	**3.10 ± 0.37**	2.51 ± 0.21	**21 ± 4**	0.90 ± 0.06	98.4%
338	1105.6	**1.90 ± 0.32**	**5.00 ± 0.74**	3.71 ± 0.41	**25 ± 5**	1.60 ± 0.13	94.4%
338	1111.6	1.70 ± 0.31	2.80 ± 0.64	2.43 ± 0.40	20 ± 7	1.30 ± 0.16	70.2%
338	1117.6	**1.70 ± 0.32**	**4.20 ± 0.72**	3.41 ± 0.41	**19 ± 4**	1.40 ± 0.12	95.4%
338	1123.6	**1.00 ± 0.31**	**3.40 ± 0.67**	2.92 ± 0.44	12 ± 6	1.15 ± 0.12	56.1%
338	1133.7	**1.80 ± 0.21**	**4.10 ± 0.61**	3.26 ± 0.37	**22 ± 3**	1.25 ± 0.09	27.1%
340	1170.1	1.40 ± 0.31	3.70 ± 0.72	3.09 ± 0.45	**16 ± 5**	1.20 ± 0.13	61.5%
340	1209.1	**1.60 ± 0.25**	**4.00 ± 0.73**	3.04 ± 0.45	**24 ± 5**	1.40 ± 0.15	70.5%
340	1234.0	**1.60 ± 0.20**	**3.50 ± 0.50**	2.84 ± 0.30	**21 ± 3**	1.40 ± 0.11	51.3%
342	1249.5	1.40 ± 0.26	3.00 ± 0.66	2.47 ± 0.39	20 ± 7	1.20 ± 0.16	19.4%
342	1264.6	**2.00 ± 0.29**	**5.10 ± 0.81**	3.81 ± 0.46	**25 ± 4**	1.30 ± 0.11	80.0%
342	1281.1	1.60 ± 0.24	3.10 ± 0.53	2.60 ± 0.34	**20 ± 5**	0.80 ± 0.08	34.1%
342	1296.4	**1.50 ± 0.17**	**3.30 ± 0.45**	2.70 ± 0.28	**20 ± 4**	1.10 ± 0.09	76.7%
343	1306.9	**1.60 ± 0.25**	**4.00 ± 0.76**	3.20 ± 0.45	**20 ± 3**	1.15 ± 0.11	49.8%
343	1317.5	1.50 ± 0.24	3.60 ± 0.77	2.83 ± 0.46	**22 ± 4**	1.05 ± 0.12	67.4%

Table 2. (continued)

Sols	Odometry (m)	Top Water (wt %)	Bottom Water (wt %)	Average Water (wt %)	Top Layer Thickness (cm)	Absorption Equivalent Chlorine (wt %)	Probability of Model Acceptance
343	1330.1	**1.40 ± 0.25**	**4.00 ± 0.51**	3.26 ± 0.29	**17 ± 4**	1.25 ± 0.09	92.7%
344	1354.7	1.20 ± 0.15	2.20 ± 0.53	1.72 ± 0.29	**29 ± 7**	0.80 ± 0.08	80.1%
344	1381.3	1.00 ± 0.14	1.80 ± 0.50	1.63 ± 0.27	13 ± 7	1.05 ± 0.13	35.0%
344	1400.2	**1.60 ± 0.16**	**3.50 ± 0.42**	2.84 ± 0.26	**21 ± 3**	1.25 ± 0.08	61.2%
345	1419.6	1.30 ± 0.15	2.70 ± 0.58	2.00 ± 0.33	**30 ± 4**	1.25 ± 0.14	37.1%
345	1438.1	**1.70 ± 0.28**	**6.00 ± 0.82**	3.99 ± 0.44	**28 ± 4**	1.10 ± 0.12	20.5%
345	1456.6	1.00 ± 0.11	2.70 ± 0.72	2.13 ± 0.40	**20 ± 3**	0.80 ± 0.05	67.0%
345	1470.3	**1.00 ± 0.07**	**5.30 ± 0.51**	3.37 ± 0.29	**27 ± 2**	1.30 ± 0.09	46.5%
347	1486.9	1.00 ± 0.13	2.80 ± 0.59	1.90 ± 0.31	**30 ± 2**	1.10 ± 0.09	78.1%
347	1503.4	1.50 ± 0.20	2.90 ± 0.61	2.43 ± 0.36	**20 ± 6**	1.45 ± 0.15	54.8%
347	1519.9	1.70 ± 0.22	3.00 ± 0.77	2.35 ± 0.45	**30 ± 5**	1.20 ± 0.12	87.7%
347	1530.5	**1.60 ± 0.18**	**3.30 ± 0.40**	2.73 ± 0.25	**20 ± 3**	1.20 ± 0.09	58.8%
349	1553.0	**1.30 ± 0.21**	**3.50 ± 0.59**	2.77 ± 0.36	**20 ± 3**	1.05 ± 0.11	72.4%
349	1569.5	1.50 ± 0.21	2.90 ± 0.60	2.39 ± 0.36	**22 ± 6**	1.15 ± 0.14	47.4%
349	1586.0	1.60 ± 0.22	3.20 ± 0.85	2.56 ± 0.49	**24 ± 4**	1.45 ± 0.13	82.2%
349	1600.6	**1.50 ± 0.22**	**3.10 ± 0.45**	2.62 ± 0.25	18 ± 6	0.90 ± 0.07	66.2%
351	1623.6	1.20 ± 0.15	2.80 ± 0.56	2.08 ± 0.29	**27 ± 5**	1.10 ± 0.12	97.1%
351	1646.2	1.20 ± 0.14	2.70 ± 0.54	2.00 ± 0.28	**28 ± 4**	1.10 ± 0.13	80.7%
351	1668.7	1.20 ± 0.15	3.20 ± 0.72	2.40 ± 0.38	**24 ± 5**	1.30 ± 0.14	35.0%
351	1685.7	1.80 ± 0.18	3.30 ± 0.49	2.58 ± 0.28	**29 ± 5**	1.10 ± 0.08	59.2%
354	1702.2	**1.70 ± 0.22**	**4.00 ± 0.73**	3.08 ± 0.50	**24 ± 5**	1.25 ± 0.14	8.2%
354	1718.8	**1.10 ± 0.23**	**3.70 ± 0.75**	2.96 ± 0.44	**17 ± 5**	1.10 ± 0.12	74.4%
354	1737.4	1.40 ± 0.25	3.40 ± 0.70	2.70 ± 0.41	**21 ± 4**	0.95 ± 0.12	68.4%
354	1742.8	**1.50 ± 0.18**	**3.60 ± 0.47**	2.55 ± 0.26	**30 ± 4**	0.85 ± 0.08	45.7%
356	1755.7	**1.00 ± 0.38**	**5.50 ± 0.59**	4.38 ± 0.37	**15 ± 3**	1.10 ± 0.09	16.5%
356	1770.2	**2.00 ± 0.20**	**5.10 ± 0.89**	3.81 ± 0.48	**25 ± 3**	1.55 ± 0.13	66.2%
356	1784.8	1.30 ± 0.24	2.10 ± 0.44	1.71 ± 0.25	**29 ± 8**	1.10 ± 0.15	79.8%
356	1792.8	**1.20 ± 0.14**	**2.40 ± 0.31**	2.00 ± 0.18	**20 ± 4**	1.05 ± 0.08	97.1%
358	1805.4	1.00 ± 0.18	2.00 ± 0.34	1.75 ± 0.21	**15 ± 4**	0.90 ± 0.08	65.8%
358	1817.9	1.30 ± 0.17	2.20 ± 0.49	1.90 ± 0.29	**20 ± 5**	1.10 ± 0.13	70.9%
358	1827.9	**1.30 ± 0.15**	**2.60 ± 0.36**	2.17 ± 0.21	**20 ± 5**	1.30 ± 0.10	93.1%
361	1850.4	**1.50 ± 0.20**	**4.00 ± 0.66**	2.96 ± 0.38	**25 ± 4**	1.20 ± 0.12	92.7%
361	1867.2	**1.30 ± 0.15**	**3.70 ± 0.67**	2.70 ± 0.39	**25 ± 3**	1.00 ± 0.10	61.5%
361	1883.8	2.30 ± 0.35	4.00 ± 0.71	3.58 ± 0.43	15 ± 8	1.65 ± 0.10	17.8%
361	1900.9	**1.50 ± 0.16**	**3.00 ± 0.43**	2.25 ± 0.23	**30 ± 5**	0.95 ± 0.11	18.6%

[a]The marks (1) and (2) in the column (2) of Table 2 indicate particular testing spots, which are associated with sampling operations at the Rocknest and drilling operations at John Klein and Cumberland (see section 5 below). The mark (3) indicates the testing spots, which were studied in the special "DAN compaign" of MSL rover [see *Litvak et al*., 2014].

There is no simple and commonly accepted method to determine the errors of the best fit parameters that are determined from the condition of the minimum of expression (6) for the data of a particular testing spot. Generally speaking, there should be some volume around the best fitting point in the parameter space, which represents the uncertainties of their values for some accepted level of confidence [e.g., see *Lampton et al*., 1976]. *Litvak et al*. [2014] suggested a straightforward method based on Monte Carlo simulations of data for each individual testing spot. In this case, the error of each parameter is the sample variance of all obtained best fitting values for this parameter, which have been found by the procedure used for the model testing. We use this method for the data in Table 2 because we believe that it properly takes into account all uncertainties of our procedure.

Formally speaking, all 152 testing spots are described by the two-layer model with different values for the water content in the top and bottom layers. However, not all of them are physically distinct from a single-layer case. One may suggest two criteria for so-called *strong two-layer models*, when the vertical water distribution is, statistically speaking, significantly distinct from the simpler single-layer model description. The *water variation criterion* is the first one: the difference $\Delta\xi_W = \xi_W^{(\mathrm{bottom})} - \xi_W^{(\mathrm{top})}$ between the water content of the bottom layer and the top layer should be larger than 3σ uncertainty of $\Delta\xi_W$. There are 50 locations in Table 2 that have a significant difference in water content between the bottom and top layers (they are shown in bold in columns

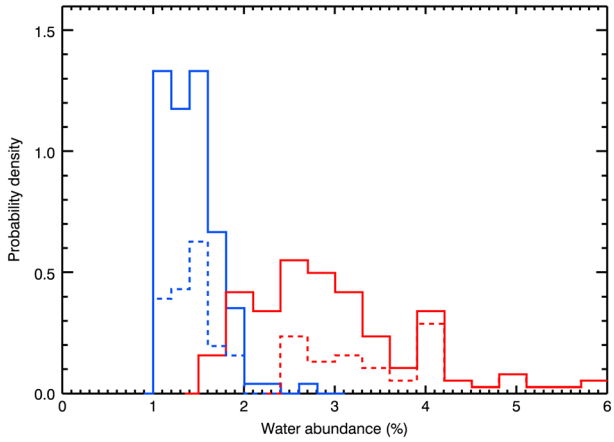

Figure 6. Distributions of $\xi_W^{(top)}$ (blue) and $\xi_W^{(bottom)}$ (red) for testing spots with direct two-layer distribution of subsurface water (models *MG4*). The distributions for strong cases of two-layer model are shown by dashed line.

(3) and (4) of Table 2). The *water depth criterion* is the second one: the thickness of the top layer, h, should be significantly larger than 3σ uncertainty of this value. Indeed, if the thickness of the top layer is not different from zero, one should not consider that location to be two layers. There are 89 spots that satisfy the second criteria (they are shown in bold in column (6) of Table 2). Convolving these two criteria, one finds 45 *strong cases* of locations with two distinct layers, which are unequivocally distinct from cases with uniform water content.

The overwhelming majority of all testing spots correspond to the so-called *direct* two-layer model of water in the subsurface: the top layer has less water than the bottom layer. The term *direct* is used for these cases because less water is expected to be in the uppermost layer due to solar irradiation and interaction with the atmosphere. The distributions of the values of $\xi_W^{(*)(top)}$, $\xi_W^{(*)(bottom)}$, and $h^{(*)}$ are presented in Figures 6 and 7. The mean content of water in the top and bottom layers are 1.5 and 3.7 wt % WEH, respectively. The difference between the water content in the top and bottom layer is about 2.2 wt % WEH, and the average thickness of the drier top layer is about 23 cm. All locations that are strong cases of the two-layer model correspond to the direct model. The WEH distributions for the strong case two-layer locations are shown by dotted lines (Figures 6 and 7).

There are 22 testing spots (14% of the total number) that have an *inverse* distribution of water in the subsurface: the water content in the top layer $\xi_W^{(*)(top)}$ is larger than $\xi_W^{(*)(bottom)}$ in the bottom layer. There are no strong two-layer cases for spots with an inverse water distribution. Only one location comes close to meeting the first criterion for the strong case: the spot with an odometry of 490 m has a difference of 2.0 ± 0.67 wt % between the top and the bottom layers. While this difference is marginally significant with 3σ confidence, the spot is unique in this respect.

A strong argument for the inverse water distribution being real is the localization of this property along the traverse: The inverse water distribution is observed in two distinct segments along the traverse: within the first 100 m from the landing site and between 455 and 638 m of odometry. One may suspect that the geomorphology of the surface in these segments of the traverse is somehow different from other regions along the traverse. The second segment contains the Rocknest site, which is the area of accumulation of aeolian sediments (see section 4 below).

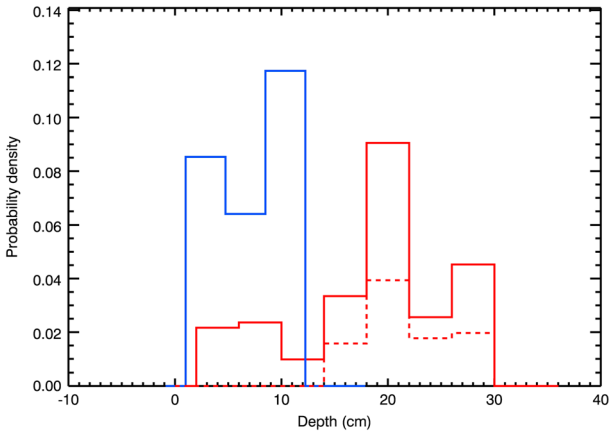

Figure 7. Distribution of thickness of the top layer h for direct (red) and inverse (blue) two-layer models (*MG4*). The distribution for strong cases of direct two-layer model is shown by dashed line.

Figures 7 and 8 present distributions of water in the top and bottom layers as well as the thickness of the top layer. The thickness of the top layer is less than 11 cm for spots having an inverse distribution. This is smaller than the thickness (about half) of the top layer for the majority of cases having a direct distribution. One cannot explain the difference between direct and inverse cases from variations in chlorine or another neutron absorbing elements because there is

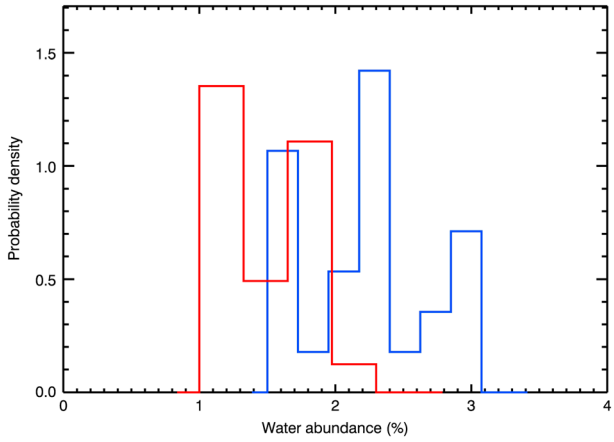

Figure 8. Distributions of $\xi_W^{(*)(\mathrm{top})}$ (blue) and $\xi_W^{(*)(\mathrm{bottom})}$ (red) for testing spots with inverse two-layer distribution of subsurface water (models *MG4*).

no statistically significant difference in absorption equivalent chlorine content for locations having either direct or inverse distributions of water (Figure 9). One has to find physical reasons for this difference, some of which will be discussed in the next section.

Figures 10–13 present the variations of water and absorption equivalent chlorine along the traverse. The shown scatterplots should not be considered to be *physical profiles* of spatial variations of the soil parameters. While a single testing spot corresponds to an area of about 3 m size, the odometry distance between individual spots varies, usually from a few meters up to tens of meters. Using the data measured at two neighboring locations separated by a distance >3 m, one should not interpolate to find the water and absorption equivalent chlorine at intermediate spots because these properties may not vary continuously. However, taking into account the special interest in the community for knowing the scale of physical variations of water and absorption equivalent chlorine in the subsurface, a special set of 18 measurements were acquired at the contact area between Sheepbed and Gillespie Lake members of the Yellowknife Bay formation ("DAN campaign", odometry from 751.4 to 764.7 m, see Table 2). In acquiring this data set the rover was moving with regular stops having a distance of only several meters between sampling locations. From the data, one can obtain the one dimensional distance profile of measured parameters (see *Litvak et al.* [2014] for details).

Except for the limited data set for "DAN campaign" in the odometry range of 13.3 m, the DAN data presented here are not sufficient to characterize the meter-scale variations of water and absorption equivalent chlorine in the soil due to limited sampling along the rover traverse. However, one can determine the large-scale phenomena in these data, which represents the extended geomorphological properties of the crater floor, for which scales are more than tens of meters. Indeed, there are clear distinctions in the water content for the four odometry ranges of 0–455 m, 455–638 m, 638–876 m, and 876–1900 m (see Figures 10–13). Table 3 presents the mean values of estimated soil parameters for these odometry ranges. First, one should note that the mean content of absorption equivalent chlorine stays practically the same for all four selected ranges: it is within the range of 1.1–1.2 wt %. Therefore, one cannot explain the variations of the mean water content parameters between these ranges by effects due to the differences of neutron absorption. Second, the range of 455–648 m has soil with a rather small vertical-average water content of about 1.47 ± 0.03 wt % WEH, and locations in this range mainly correspond to the inverse two-layer model marked by decreasing water profile with depth. Third, there exists a similarity of the water layering in the ranges 0–455 m, 671–876 m, and 876–1900 m: the direct two-layer models fit the data in these ranges and with practically the same water content in the top layer, 1.5–1.7 wt % WEH. The major difference between these three ranges is the water content in the bottom layer: the mean water in the bottom layer increases from 2.2 ± 0.1 wt % WEH in the first range up to 3.3 ± 0.1 wt % WEH in the last, an increase of 50% of the modeled value.

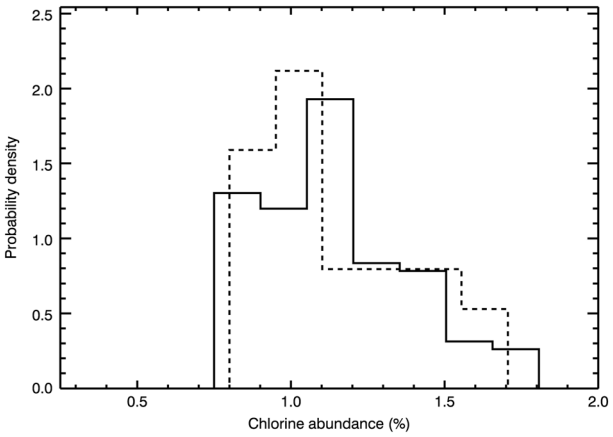

Figure 9. Distributions of absorption equivalent chlorine content $\xi_{\mathrm{Cl}}^{(*)}$ for testing spots with direct (solid line) and inverse (dashed line) distribution of water (models *MG4*).

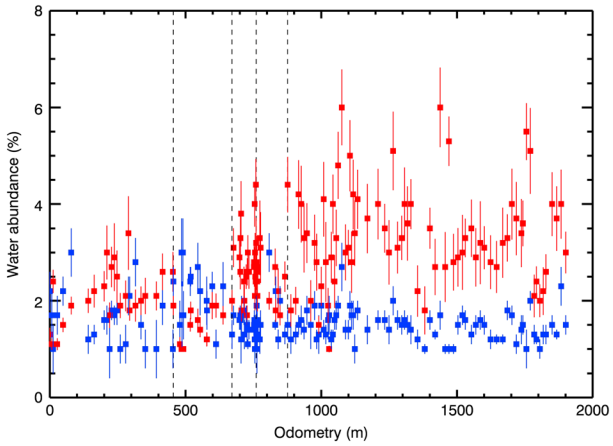

Figure 10. Variations of estimated content of water at top $\xi_W^{(*)(\mathrm{top})}$ (blue) and bottom $\xi_W^{(*)(\mathrm{bottom})}$ (red) layers along the traverse (models *MG4*). Dashed lines indicate the boundaries of odometry ranges, as presented in the Table 3.

5. DAN Measurements for Three Sampling Sites

Two sites, named John Klein and Cumberland, inside the Sheepbed member were selected for the first drilling operations on the Martian surface [*Ming et al.*, 2013]. The mineralogical data from the CheMin XRD instrument have revealed a significant component of phyllosilicates, ~20% abundance, from the John Klein and Cumberland drill samples [see *Vaniman et al.*, 2013].

The DAN campaign was initiated immediately after the accomplishment of drilling and sample analysis operations at the Cumberland site. On sol 295 Curiosity executed a U- turn in-place to make DAN measurements with the instrument directly above the John Klein and then Cumberland drilling sites. The estimated soil parameters for measurements at John Klein and Cumberland sites are presented in Table 2 for odometry of 729.5 and 733.5 m, respectively. There are strong cases of direct two-layer models at these sites with large difference of water content (1.2–1.9 wt % WEH) between the bottoms and the top layers of the subsurface. It is interesting to compare these results with the data for another site of soil sampling, the Rocknest sand shadow. This site of accumulation of aeolian sediment was selected for the first Curiosity sampling operations (scooping the top several centimeters of the surface). For the odometry range within the Rocknest location, from 485.1 to 491.9 m, the DAN data indicate that the soil has the lowest content of detected water among all presented testing spots, about 1 wt % WEH (see Table 2).

It is interesting to compare DAN results obtained at the Rocknest sampling area and at the drilling sites in Yellowknife Bay formation with SAM and APXS measurements made at the same locations (Table 4). SAM and APXS have analyzed soil material excavated from the boreholes at depths of 6.5 cm. SAM searches for volatiles released using evolved gas analysis [*Mahaffy et al.*, 2012]. The major evolved gases from the drill samples are H_2O, CO_2, SO_2, and O_2. The analysis of low-temperature water release has revealed that water content in the John Klein samples ranged between 1.6 and 2.5 wt % and water content in the Cumberland samples ranged between 1.0 and 2.3 wt % [*Ming et al.*, 2013]. The APXS measurements of chlorine abundances show the presence of ~0.7% at John Klein and ~1.4% at Cumberland [*Vaniman et al.*, 2013].

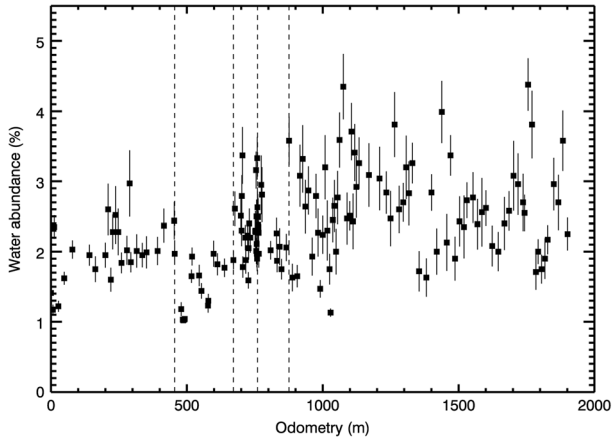

Figure 11. Variations of estimated average content of water $\xi_W^{(\mathrm{av})}$ along the traverse (models *MG4*). Dashed lines indicate the boundaries of odometry ranges, as presented in the Table 3.

DAN, SAM, and APXS measurements at all sampling locations are summarized in Table 4. They are in good agreement at Rocknest, where DAN estimation of water at the top layer is similar to the value from SAM, and DAN estimation of absorption equivalent chlorine is also similar to the value from APXS [*Blake et al.*, 2013]. Moreover, one may conclude that the data from SAM are consistent with the inverse model of water distribution (decreasing with depth) found by DAN at Rocknest. Indeed, the DAN data indicate a very small average in-depth content of water about 1 wt % WEH, and the only model tested here that reaches agreement with

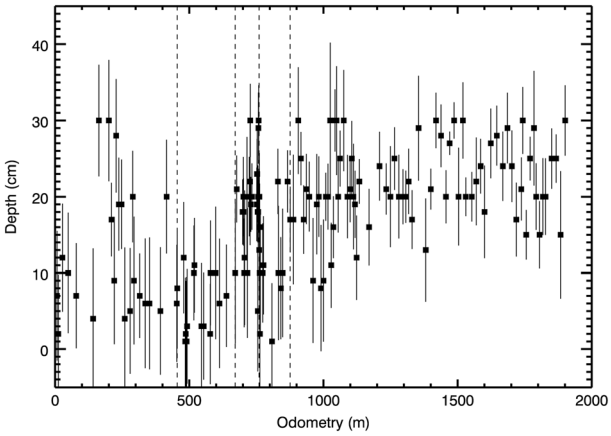

Figure 12. Variations of estimated thickness of the top layer of two-layer models *MG4*.

the SAM value is the inverse two-layer model with ~2 wt % WEH of water in the uppermost layer.

For both drilling sites, John Klein and Cumberland, there is rather good agreement between DAN and APXS for chlorine, and between DAN and SAM for water (Table 4). The average water content 2.2–2.4 wt % WEH found by DAN at John Klain and Cumberland sites is also consistent with 20 wt % phyllosilicate abundance found by ChemMin [*Vanuman et al*. 2013]. The content of water in phylloosilicates is thought to be about 10 wt %, so the product of these two fractions leads to the bulk water content of ~2 wt %, in agreement with DAN.

Some observed differences between the values based on DAN, a remote sensing instrument, versus SAM and APXS, which are contact and direct analysis instruments, should not be considered problematic. The probing mass for DAN is orders of magnitude larger than the mass analyzed by SAM and APXS. In this sense, the remote sensing observations by DAN and the direct analysis by SAM and APXS are highly complementary and provide important information at multiple scales.

6. Discussions and Conclusions

The Martian soil contains water in three distinct forms: the first form is water structurally bound inside minerals (chemically bound water), the second form consists of water molecules adsorbed in multilayers over the surface of regolith grains (adsorbed water), and the third form is free water ice in the porous volume of the regolith. The third form of water is not stable in the upper most layer of subsurface at the latitude of Gale and is subject to sublimation, so one should focus on the first and on the second potential reservoirs. According to the DAN data, the majority of testing spots along the initial 1900 m of Curiosity's traverse have the so-called direct water distribution, where a drier top layer, with about 1.5–1.7 wt % WEH of water, lies above a wetter bottom layer with about 2.2–3.3 wt % WEH of water (see Tables 2 and 3).

The thickness of the top layer is about 10–20 cm, which is consistent with the thermal skin depth for diurnal temperature variations (1–20 cm depending on the type of soil) [see, for example, *Mellon et al*. 2004; *Putzig and Mellon*, 2007]. Therefore, one may suggest that the top layer has less water due to diurnal and seasonal temperature variations as a result of enhanced interaction with the Martian atmosphere. Only chemically bound water and some absorbed water might reside in the top layer under these conditions, and this investigation suggests that the abundance is equivalent to about 1.5 to 1.7 wt % WEH water (see Tables 2 and 3). The bottom layer is more isolated from the thermal wave and from the atmosphere, and the soil of this layer may contain more adsorbed water on the surface of grains or higher hydrated

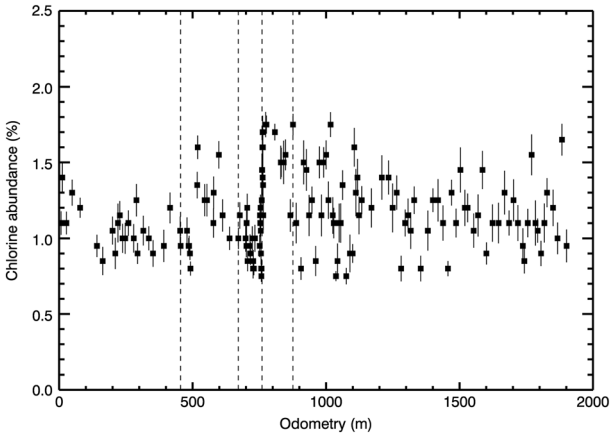

Figure 13. Variations of estimated content of absorption equivalent chlorine $\xi_{Cl}^{(*)}$ along the traverse.

Table 3. Average Parameters of Soil for Four Different Ranges of the Curiosity Odometry

Odometry Ranges	0–455 m	455–638 m	638–876 m	876–1900 m
(1)	(2)	(3)	(4)	(5)
Top water (wt %)	1.68 ± 0.08	2.17 ± 0.12	1.50 ± 0.04	1.48 ± 0.03
Bottom water (wt %)	2.23 ± 0.08	1.41 ± 0.04	2.64 ± 0.06	3.33 ± 0.07
Vertical-average water (wt %)	2.07 ± 0.05	1.47 ± 0.03	2.31 ± 0.04	2.65 ± 0.04
Thickness of thetop layer (cm)	13 ± 1	6 ± 2	16 ± 1	22 ± 1
Content of absorption equivalent chlorine (wt %)	1.07 ± 0.02	1.14 ± 0.02	1.19 ± 0.01	1.17 ± 0.01

forms of minerals that are more stable under these conditions. Using the mean values for the testing spots with direct two-layer models (Table 3), one may estimate that the bottom layer might have an additional 0.7–1.6 wt % WEH of adsorbed water. Unfortunately, the Curiosity rover does not have the capability to test the direct two-layer distribution model of ground water: according to DAN data, the bottom layer with larger water abundance is at the depth of 10–20 cm, which is not accessible to the rover's tools.

In the odometry range of 455–671 m (see Table 3) the DAN data support the inverse two-layer model with larger water content in the top of the soil. Its thickness is only a few centimeters, which is at the limit of DAN sensitivity for detection of a layered deposit. The dominance of the inverse two-layer model for testing spots along this particular range of the traverse supports its reality and suggests it is not merely an artifact of the tested model group (see Table 2). The Rocknest area of aeolian sediment lies in this odometry range, which have exceptionally small water contents at the bottom layer (1.0 wt %) and the exceptionally high content of water at the top layer (3.0 wt %, odometry position of 490 m, see Table 2). As a possible physical explanation of the phenomenon of inverse two-layer water distribution one may suggest that DAN detected some additional component of increased hydration (~2–3 wt % WEH) in the uppermost layer. This material would cover the typical soil, having a water content of about 1.5–1.7 wt %, which is rather similar to the estimated water content of the top layers at testing spots with direct two-layer distribution (Table 3). The larger water content in the upper soil could be either related to a larger fraction of hydrated minerals or with a larger specific surface area of aeolian sediments. More data are necessary to understand the phenomenon of the inverse two-layer water distribution: one hopes that more locations can be found with this unusual property, from which data may provide some additional key knowledge for a successful interpretation.

Perhaps the largest surprise of the current data analysis is the relatively small content of water that typifies the soil along the traverse. For the odometry ranges consistent with the direct two-layer model, the vertical-average water in the subsurface is about 2.1–2.7 wt % WEH (Table 3). These values for water content based on DAN data are about 2 times smaller than the value about 5 wt % WEH in the area of Gale Crater deduced from the orbital data of the Gamma-Ray Spectrometer (GRS) suite of instruments on board the NASA Mars Odyssey spacecraft [see *Mitrofanov et al.*, 2014]. The simplest possibility to explain this discrepancy is based on the assumption that DAN data represent a much smaller linear scale (about 2 km of odometry) compared with the field of view of the Mars Odyssey instruments (for High Energy Neutron Detector (HEND), for example, the radius of field of view is about 300 km). The alternative explanation of the discrepancy suggests that HEND sees much deeper subsurface than DAN does, 1 m versus 60 cm, and HEND data may indicate that materials below 60 cm contain more water than materials above this depth. Using a two-layer model for HEND data analysis, one finds for the area of Gale Crater a water abundance of 6–8 wt % below the top "dry" layer with the thickness of 10–16 cm. Continued measurements by DAN on board Curiosity during the trek to Mount Sharp will allow continued testing of these models for more accurate comparison to orbitally acquired HEND data.

Table 4. Comparison of DAN, SAM, and APXS Data for Three Sampling Sites

	Comparison of Water					Comparison of Chlorine	
Sampling Sites	SAM Water (wt %)	DAN Top Water (wt %)	DAN Depth (cm)	DAN Bottom Water (wt %)	DAN Averge Water (wt %)	APXS Cl (wt %)	DAN Absorption Equivalent Chlorine (wt %)
Rocknest	2	2.2 ± 0.3	4 ± 4	1.0 ± 0.04	1.1 ± 0.04	1	0.9 ± 0.04
John Klein	1.6–2.5	1.10 ± 0.14	19 ± 4	3.0 ± 0.4	2.4 ± 0.2	0.7	0.79 ± 0.04
Cumberland	1.0–2.3	1.40 ± 0.17	20 ± 4	2.6 ± 0.4	2.2 ± 0.2	1.4	1.06 ± 0.09

Acknowledgments

The DAN team is thankful to the highly professional MSL project team members who have maximized opportunities for DAN measurements on Mars. The DAN team very much appreciates the work of colleagues from the N. L. Dukhov Institute for Automatics for the development of the reliable PNG for this experiment. Also, the DAN team appreciates the valuable cooperative support of two national space agencies, Roscosmos and NASA, which, working together, have made this Russian-contributed instrument possible on an American rover. Finally, the team thanks the Curiosity science community, which provided essential comments and advice to the DAN team during numerous discussions. This work is partially supported by the grant # 14-22-00249 from Russian Science Foundation.

References

Blake, D., et al. (2013), Curiosity at Gale Crater, Mars: Characterization and analysis of the Rocknest sand shadow, *Science*, *341*, doi:10.1126/science.1239505.

Brückner, J., et al. (2008), Mars Exploration Rovers: Chemical composition by the APXS, in *The Martian Surface: Composition, Mineralogy, and Physical Properties*, edited by J. Bell, pp. 58–101, Cambridge Univ. Press, New York.

Grotzinger, J. P., et al. (2012), Mars science laboratory mission and science investigation, *Space Sci. Rev.*, *170*, 5–56, doi:10.1007/s11214-012-9892-2.

Hardgrove, C., J. Moersch, and D. Drake (2011), Effects of geochemical composition on neutron die-away measurements: Implications for Mars science laboratory's dynamic Albedo of neutrons experiment, *Nucl. Instrum. Methods Phys. Res. A*, *659*(1), 442–455.

Jun, I., et al. (2013), Neutron background environment measured by the Mars Science Laboratory's Dynamic Albedo of Neutrons instrument during the first 100 sols, *J. Geophys. Res. Planets*, *118*, 2400–2412, doi:10.1002/2013JE004510.

Lampton, M., B. Margon, and S. Bowyer (1976), Parameter estimation in X-ray astronomy, *Astrophys. J.*, *208*, 177–190.

Litvak, M. L., et al. (2008), The Dynamic Albedo of Neutrons (DAN) Experiment NASA's 2009 Mars Science Laboratory, *Astrobiology*, *8*(3), 605–612.

Litvak, M. L., et al. (2014), Local variations of bulk hydrogen and chlorine-equivalent neutron absorption content measured at the contact between the Sheepbed and Gillespie Lake units in Yellowknife Bay, Gale Crater, using the DAN instrument onboard Curiosity, *J. Geophys. Res. Planets*, *119*, doi:10.1002/2013JE004556.

Mahaffy, P. R., et al. (2012), The sample analysis at Mars investigation and instrument suite, *Space Sci. Rev.*, *170*, 401–478, doi:10.1007/s11214-012-9879-z.

Mellon, M. T., W. C. Feldman, and T. H. Prettyman (2004), The presence and stability of ground ice in the southern hemisphere of Mars, *Icarus*, *169*, 324–340, doi:10.1016/j.icarus.2003.10.022.

Ming, D. W., et al. (2013), Organic, volatile, and isotopic compositions of a sedimentary rock in Yellowknife Bay, Gale Crater, Mars, *Science*, doi:10.1126/science.1245267.

Mitrofanov, I. G., et al. (2012), Experiment for measurements of Dynamic Albedo of Neutrons (DAN) onboard NASA's Mars Science Laboratory, *Space Sci. Rev.*, *170*(1–4), 559–582.

Mitrofanov, I. G., et al. (2014), Studying of water content in Mars' Gale Crater: The first results of the DAN experiment on the NASA curiosity rover, Doklady Physics, *Russ. Acad. Sci.*, *455*(3), 1–3.

Putzig, N. E., and M. T. Mellon (2007), Apparent thermal inertia and the surface heterogeneity of Mars, *Icarus*, *191*(1), 68–94.

Vaniman, D. T., et al. (2013), Mineralogy of a mudstone at Yellowknife Bay, Gale Crater, Mars, *Science*, *343*(6169), doi:10.1126/science.1243480.